Journal of the Oceanographical Society of Japan
Vol. 40, pp. 303 to 313, 1984

A Coupled Discrete Wave Model MRI-II*

Takeshi Uji†

Abstract: An ocean wind-wave prediction model MRI-II is developed on the basis of the energy balance equation which contains five energy transfer processes, namely, the input by the wind, the nonlinear transfer among the components of windsea by resonant wave-wave interactions, wave breaking, frictional dissipation and the effect of opposing winds.

The nonlinear energy transfer is expressed implicitly together with the wind effect by Toba's one-parameter representation of windsea, but neither swell-swell nor swell-windsea resonant interactions are considered.

Hypothetical assumptions are introduced to describe wave breaking effects. The numerical constant required in the assumptions of wave breaking is determined through trial test runs for a hindcast performed on the North-western Pacific Ocean.

The significant wave height, one-dimensional wave spectrum and two-dimensional wave spectrum hindcasted by this new model are in more reasonable agreement with observations than those obtained with our old model MRI.

1. Introduction

The evolution of a surface wave field in space and time is governed by the energy balance equation

$$dF/dt=\partial F/\partial t+\boldsymbol{Cg}\cdot\nabla F = S_{net}=S_{in}+S_{nl}+S_{ds}\,, \qquad (1)$$

where $F(\sigma,\theta';\ x,t)$ is the two-dimensional wave spectrum, dependent on angular frequency σ and propagation direction θ', $\boldsymbol{Cg}=\boldsymbol{Cg}(\sigma,\theta')$ is the group velocity, ∇ is the gradient operator in the horizontal plane and the net source function S_{net} is represented as the sum of the input S_{in} by the wind, the non-linear transfer S_{nl} and the dissipation S_{ds}.

We developed an operational wave model (wave model here means ocean wave prediction model) called MRI (Meteorological Research Institute) based on Eq. (1) (Uji and Isozaki, 1972; Isozaki and Uji, 1973; Uji, 1975) and it has been used for routine wave forecasting at the Japan Meteorological Agency since 1977. The model MRI contains four energy transfer processes, namely, linear and exponential wave growth, wave breaking leading to an equilibrium state of Pierson-Moskowitz spectrum, frictional dissipation for over-saturated waves and decay of waves due to opposing winds. Since no wave-wave interactions are considered in this model, evolution of the spectral component of waves is completely mutually independent.

The intercomparison of wave models carried out in 1981 by the Sea Wave Modelling Project (SWAMP) Group made it clear that MRI is inferior in predicting the spectral form for early growth stages, while superior in predicting waves for complicated winds such as hurricanes relative to the other models based on the parametric representation of windsea (The SWAMP Group, 1982a, 1982b).

This report describes a new wave model which was developed to overcome the weaknesses of MRI without losing its merit by incorporating recent physical pictures of windsea growth and a hypothetical representation of the wave breaking effect.

Of particular importance to our new model are the following works. Toba (1972, 1973a, 1973b) introduced the hypothesis of local balance and proposed the existence of a 2/3 power law between wave height and period. He also proposed a single-parameter formula for the growth of windsea (Toba, 1978). Hasselmann *et al.*

* Received 21 December 1983; in revised form 21 April 1984; accepted 7 May 1984.

† Meteorological Research Institute, 1-1, Nagamine, Yatabe-Machi, Tsukuba-gun, Ibaraki 305, Japan.

(1973) observed windsea growth, studied wave-wave resonant interactions theoretically analyzed by Hasselmann (1962) for the observed spectra, and proposed a spectral form called the JONSWAP spectrum. Recently Mitsuyasu *et al.* (1980) carefully examined the spectra of growing windsea in the ocean and found relations between the fetch and parameters in the JONSWAP spectrum. These parametric representations of windsea growth provide a new basis for developing wave models and are useful in improving the weak points of MRI.

Fairly detailed empirical knowledge is available about the frequency spectrum of the fetch-limited windsea. Some problems, however, are left unsolved for wave models. First, we still do not have full understanding of the energy transfer from wind to waves. Second, the energy transfer between swell and windsea cannot as yet be incorporated explicitly in models, because the exact computations for the nonlinear energy transfer function S_{nl} are still too time consuming to carry out. Third, we know little about the dissipation of energy due to wave breaking. Therefore, a wave model necessarily has to introduce some assumptions compensating for our partial knowledge so that the model is useful under any operational conditions. For this reason we introduce some assumptions to express the dissipation of energy due to wave breaking in MRI-II.

In MRI, the spectrum is represented as a two-dimensional discrete array of frequency-direction energy "packets", each of which propagates at its appropriate group velocity. The advantage of MRI mainly comes from this flexible representation of waves under variable wind conditions, and so this representation is also used for MRI-II. A wave model incorporating a parametric description of windsea along with discrete spectral representation of the entire spectrum, including both windsea and swell, is referred to as a coupled discrete (CD) model by the SWAMP Group. Thus, MRI-II is classified as a CD wave model.

In the next section, the spectral form of the windsea and the form of the dissipation function for wave breaking for MRI-II will be presented. In Section 3, a numerical constant required for wave breaking will be determined through trial test runs for a hindcast of waves due to typhoon ORCHID. In section 4, we will examine the basic performance of MRI-II in an experiment which examines the growth of a wave field for a uniform, stationary wind blowing orthogonally off a straight shore. Conclusions will be drawn in section 5.

2. Basic description of MRI-II

In this section a parametric representation of the windsea and assumptions for wave breaking are introduced and they are incorporated in Eq. (1). Variables with the suffix * at the upper right are non-dimensionalized in terms of the friction velocity u_* and the acceleration of gravity g.

2.1. Representation of windsea

We assume the following properties of windsea under a homogeneous and steady wind to obtain parametric description of the net source function S_{net}^* for growing waves:

1) the one-dimensional (frequency) spectrum of the windsea ϕ^* keeps a similar form determined by the spectral peak frequency σ_p^* and finally reaches a fully developed equilibrium state expressed by the Pierson-Moskowitz spectrum $\phi_{pm}^*(\sigma^*;\ \sigma_{pm}^*)$ at a sufficiently large fetch, *i.e.*

$$\phi^* = C_0 \phi_{pm}^* (\sigma^*;\ \sigma_p^*),$$

where C_0 is a coefficient independent of σ^*,

$$\phi_{pm}^*(\sigma^*;\ \sigma_{pm}^*) = \alpha_{pm}\sigma^{*-5} \exp(-1.25\, \sigma_{pm}^{*4}/\sigma^{*4}),$$

$\alpha_{pm}=8.1\times10^{-3}$, $\sigma_{pm}^*=(0.8\beta_0)^{1/4}\sigma_0 u_*/g$ is the peak frequency of the Pierson-Moskowitz spectrum, $\beta_0=0.74$, $\sigma_0=g/U_{19.5}$ and $U_{19.5}$ is wind speed at 19.5 m height.

2) the evolution of the parameter σ_p^* follows Toba's stochastic growth equation (Toba, 1978), *i.e.*

$$\partial\sigma_p^{*-2}/\partial t^* + (1/2\sigma_p^*)(\partial\sigma_p^{*-2}/\partial x^*) = G[1-erf(b_0\sigma_p^{*-1})], \quad (2)$$

where x^* is the fetch, $G=1.75\times10^{-3}$ and $b_0=0.044$;

3) the total energy E^* of wind waves is proportional to σ_p^* to the minus third power (Toba, 1978), *i.e.*

$$E^* \propto \sigma_p^{*-3};$$

4) the directional distribution function for a windsea spectrum is $(2/\pi)\cos^2\theta$, where θ is the angle between wind and θ'. Then the two-dimensional spectrum F^* which satisfies all of the above four assumptions is

$$F^*(\sigma^*, \theta'; \sigma_p^*) = \alpha_{pm}\sigma_p^*\sigma_{pm}^{*-1}\sigma^{*-5} \times \exp(-1.25\,\sigma_p^{*4}\sigma^{*-4})(2/\pi)\cos^2\theta . \quad (3)$$

The total energy E of this spectrum is

$$E^* = \alpha_{pm}/(5\,\sigma_{pm}^*\sigma_p^{*3}) . \quad (4)$$

2.2. Arrangement of growth equation

Since the spectral form of Eq. (3) is different from that of Toba (1978), the constants in Eq. (2) are recalculated. Wilson's (1965) formula is non-dimensionalized by use of the drag coefficient $Cd = 1.2\times10^{-3}$ for the wind velocity at 10 m height. Then, the differentiated form of it is approximated after Toba (1978) as follows

$$T_p^{*2}(dT_p^*/dx^*) = C_1[1 - erf(C_2 \cdot T_p^*)], \quad (2')$$

where $T_p^* = 2\pi/\sigma_p^* = 1.05T^*$ (Toba, 1978), T^* being the wave period and C_1 and C_2 constants. Since the ratio on the right hand side of Eq. (2') for different values of T_p^* does not depend on C_1, the value of C_2 is determined such that the ratio for two typical values of T_p^* (2.5 and 190), respectively, corresponding to the early and final growth stage be equal to the corresponding ratio given by Wilson's formula. The value so obtained for C_2 is 7.317×10^{-3}. The method of least squares in the range of T_p^* from 2.5 to 250 gives a value of $C_1 = 0.4559$ for this value of C_2.

To incorporate the fetch equation (2'), which controls the fetch-limited growth in a steady state, into Eq. (1) we have to express S_{net} by use of Eq. (2'). For this purpose we integrate Eq. (1) for all spectral components and obtain the equation,

$$\partial E/\partial t + \iint \boldsymbol{Cg}\cdot\nabla F\, d\sigma d\theta = \partial E/\partial t + \nabla(\overline{\boldsymbol{Cg}}\cdot E) = SE_{net}, \quad (5)$$

to lead a fetch equation, where

$$SE_{net} = \iint S_{net}\, d\sigma\, d\theta \text{ and}$$

$$\overline{\boldsymbol{Cg}} = \left(\iint \boldsymbol{Cg}\cdot F\, d\sigma\, d\theta\right)\Big/ E .$$

If the wind blows in the x direction and the coast line lies at right angles to x, the above equation becomes

$$d(\overline{Cgx}^*E^*)/dx^* = SE_{net}^* \quad (6)$$

for a stationary wave field, where $\overline{Cgx}^*$ is the component of $\overline{\boldsymbol{Cg}}^*$ in the x direction and

$$\overline{Cgx}^* = 0.7276\cdot Cg_p^*,$$

for the spectral form of Eq. (3), where $Cg_p^* = 1/(2\sigma_p^*)$. Eqs. (2'), (4) and (6) together with the above determined values of C_1 and C_2 give the growth equation for the parameter σ_p^*

$$d\sigma_p^{*-2}/dt^* = 1.783\times10^{-3}\,[1 - erf(4.59\times10^{-2}\,\sigma_p^{*-1})] . \quad (7)$$

Therefore, the net source function is expressed as

$$S_{net}^*\cdot\Delta t^* = F^*(\sigma_p^* + \Delta\sigma_p^*) - F^*(\sigma_p^*) , \quad (8)$$

where Δt^* is the time interval of numerical integration and $\Delta\sigma_p^*$ is the amount of change of σ_p^* given by Eq. (7) for Δt^*.

2.3. Energy dissipation for over-saturated components

For growing wind waves, S_{net} is expressed by Eq. (8). But we cannot apply it to over-saturated components. The energy dissipation S_{ds} should balance $S_{in}+S_{nl}$ for spectral components around the fully developed equilibrium level, so that we have to describe S_{ds} in terms of wind and waves. Since a swell can propagate with very small dissipation on a calm sea, the energy dissipation due to the viscosity of the water can be considered very small. Thus, energy dissipation mainly occurs through wave breaking. However, the phenomenon of wave breaking of wind waves is very irregular and complex, and no theoretical model of wave breaking is currently available. For this reason, we assume hypothetically that waves break as follows:

1) wave breaking is a process in which a water mass at a wave crest with a mass proportional to the square of the wave height loses its wave motion energy; 2) the energy dissipation for a unit area of the sea per occurrence of wave breaking is proportional to the mass of breaking water and the total energy E of waves including both windsea and swell; 3) the number of occurrences of breaking per unit time, P is expressed as

$$P=Pi\,\sigma_p\,,$$

where σ_p is the characteristic frequency which is related to the total energy including both windsea and swell by extended application of Eq. (3) to ocean waves as follows

$$\sigma_p=(\alpha_{pm}g^2/5\,\sigma_{pm}E)^{1/3}.$$

Pi is the probability of breaking, which has a value between 0 and 1 and is expressed by the empirical formula,

$$Pi=0.27\log(u_*^2/\sigma_p\nu)-0.78\,,$$

obtained for data collected by Toba (1979), where ν is the kinematic viscosity of the air.

These assumptions are summarized to yield

$$\iint S_{ds}\,d\sigma\,d\theta=-Da\cdot E \text{ and } Da=C_b\cdot P\cdot E\,,$$

where Da is the damping factor for the total energy E and C_b is a constant whose value will be determined through a case study by use of a best-fit technique.

Let Br be a damping ratio for each two-dimensional spectral component, *i.e.* $-S_{ds}=Br\cdot F$. For the expression of Br, we have to assume the following additional property:

4) the damping ratio Br depends only on frequency normalized by σ_p as

$$Br\propto(1+(\sigma/2\sigma_p)^4),$$

because our numerical experiment using artificial wave data shows that removal of a water mass from each wave crest acts on the spectrum in approximately the same way as a low-pass filter with the damping ratio constant at the low of the cut-off frequency $2\sigma_p$ but depending on the 4th power of frequency at the high frequency end. It then follows that

$$Br=Da\cdot E(1+(\sigma/2\sigma_p)^4)/E_n,$$
$$\text{where } E_n=\iint(1+(\sigma/2\sigma_p)^4)F\,d\sigma d\theta \quad (9)$$

because the relation

$$\iint Br\cdot F\,d\sigma d\theta=Da\cdot E$$

should be satisfied. Finally we obtain the expression

$$S_{ds}=-C_b\cdot Pi\cdot\sigma_p E^2(1+(\sigma/2\sigma_p)^4)F/E_n\,. \quad (10)$$

When a spectral component is nearly as large as the fully developed spectral component, $S_{in}+S_{nl}$ must be nearly equal to S_{ds} so that

$$S_{in}+S_{nl}=[(F/F_\infty)^2-2]S_{ds}$$

is assumed for the spectral component whose magnitude ranges from the fully developed level to 1.414 times this level, to satisfy the relation $-(S_{in}+S_{nl})=S_{ds}$ at the fully developed spectral level F_∞, where $F_\infty=\phi_{pm}(\sigma_{pm})\ (2/\pi)\cos^2\theta$. For wave components larger than $1.414\,F_\infty$, $S_{in}+S_{nl}$ is considered negligible compared with S_{ds}.

In MRI-II the above mentioned representation of S_{ds} results in a kind of swell-windsea interaction, because the local state of wind and windsea affects the dissipation of swell through Eq. (10). But this interaction only reduces the total energy, and is quite different from resonant wave-wave interactions which conserve the total energy.

For the waves in opposing wind, three energy dissipation effects are considered: (1) wave breaking which is assumed to be independent of the direction of wave propagation, (2) the suppressing effects of wind for waves propagating against the wind and (3) the energy dissipation due to viscosity, where the latter two effects were already introduced in MRI. The non-linear energy transfer between swell and windsea due to resonant wave-wave interactions is neglected, because we do not have yet a simple enough parametrized description of S_{nl} for all forms of wave spectrum that can be practically incorporated in a wave model.

2.4. Numerical scheme

We use the same expression of the two-dimensional spectrum and the same scheme for wave energy propagation as in MRI (Uji and Isozaki, 1972), *i.e.*, wave energy is numerically represented by 352 (16 directions times 22 frequencies) spectral components, and equally spaced grids on local Cartesian co-ordinates are employed.

Our calculation consists of the following seven steps:

1) each two-dimensional energy spectral component propagates for a given time interval Δt;

2) the damping coefficient Br due to wave breaking is determined by Eq. (9);

3) a frequency spectrum $\phi(\sigma)$ is calculated by

the method of least squares, *i.e.* the value of $\phi(\sigma)$ is determined to minimize the value of the integral

$$\int_{-\pi/2}^{\pi/2}(F(\sigma,\theta')-\phi(\sigma)(2/\pi)\cos^2\theta)^2 d\theta\ ;$$

4) the peak frequency σ_p is determined by the best fit of $\phi(\sigma;\sigma_p)$ to $\phi(\sigma)$, where the swell components are disregarded;

5) the peak frequency σ_p is transformed to the corresponding duration t using the duration-limited growth curve of σ_p obtained from Eq. (7);

6) the new windsea is given for the new time step $t+\Delta t$;

7) the evolution of non-growing components are calculated by simple time integration using the damping coefficient Br.

3. A case study and determination of the magnitude of the wave breaking effect

During the period of typhoon ORCHID (8013), sea waves were observed in three different ways: (1) with ultrasonic wave gauges set on the bottom of the sea at a depth of 50 m at coastal observation stations, (2) at the ocean data buoy No. 3 (Buoy No. 3) and (3) with a ship-borne wave recorder on the research vessel (R. V.) *Shumpu Maru*. The observation stations and

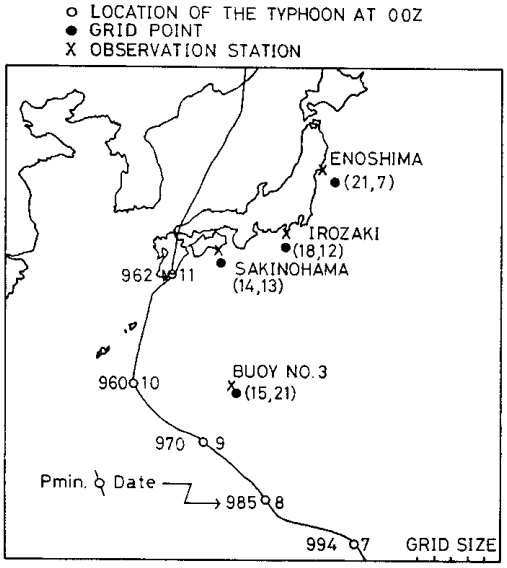

Fig. 1. The track of typhoon ORCHID (8013) and the observation stations in the area of the hindcast. The grid size, 127km, is also shown in the lower right corner.

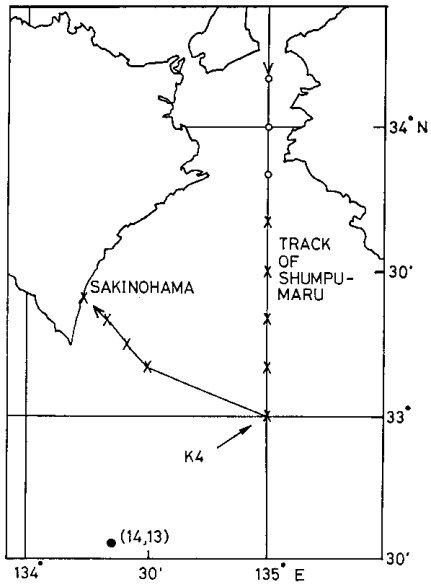

Fig. 2. The track of the R. V. *Shumpu Maru*, the Sakinohama observation station and the nearest grid point to them (solid circle). The observation stations whose data are referred to in the text are marked by crosses.

the path of the typhoon in our computation area are shown in Fig. 1, and the observation stations R.V. *Shumpu Maru* are shown in Fig. 2.

The wind field of the typhoon is given as a vector sum of the circular symmetrical wind field calculated from the pressure field expressed by Fujita's formula and the wind field parallel to the forward speed of the typhoon (Uji, 1975). The wind fields were analyzed every three hr and every 127 km from 15:00 GMT (15 z) 06 September 1980 to 12 z 13 September 1980 to carry out a hindcast of sea waves using MRI at the Maritime Meteorological Division of the Marine Department, Japan Meteorological Agency (JMA). The two-dimensional wave spectra travelling into calculation area through the boundary are determined by use of the results of the routine operation of wave prediction at JMA.

3.1. Determination of the magnitude of the wave breaking effect

The dissipation source function S_{ds} in Eq. (10) still has an undetermined dimensional constant C_b. For various values of C_b, hindcast calculations of sea waves caused by the typhoon were repeated. Obtained wave heights were

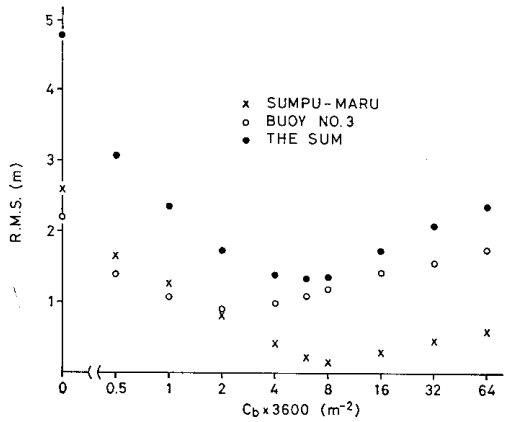

Fig. 3. Root mean squares of differences between hindcasted and observed wave heights plotted against the value of the coefficient of the dissipation term, C_b.

compared with observed ones in two ways, at Buoy No. 3 and with the R.V. *Shumpu Maru*, because observed waves at stations of these two ways are considered to be less affected by the coast line. The root mean square of 38 differences in wave height between those observed at Buoy No. 3 and those calculated at the nearest grid point (15, 21) to the buoy and the root mean square of differences between eight data collected by the R.V. *Shumpu Maru* and those at the grid point (14, 13) are plotted against the various value of C_b in Fig. 3 together with their sum. The value, $C_b=6/3600\ \mathrm{m}^{-2}$, is obtained as the best value of C_b which minimized the sum of the two root mean squares.

3.2. *Hindcasted Results*

Figure 4 compares wave heights observed at Buoy No. 3 during the period from 21 z 08 September to 12 z 13 September with those hindcasted by three wave models: (1) MRI (open circles), (2) MRI-II with no wave breaking effects (solid circles) and (3) MRI-II with the wave breaking effects (crosses). Figures 5, 6 and 7 show the same as Fig. 4 but for other observation stations.

MRI-II with no wave breaking effects consistently gives much higher wave heights than the other two wave models and actual observations through the whole period except in the early growth stages. This shows that the energy dissipation for over saturated components plays an important roll in complicated wind fields,

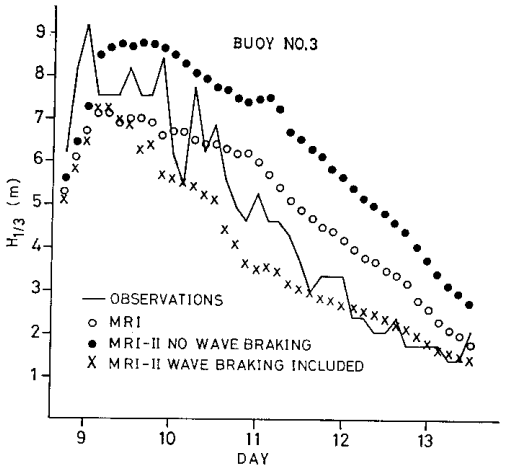

Fig. 4. Observed and computed significant wave heights at Buoy No. 3 and the grid point (12, 17). The graduation of the date on the abscissa is at every 00: GMT.

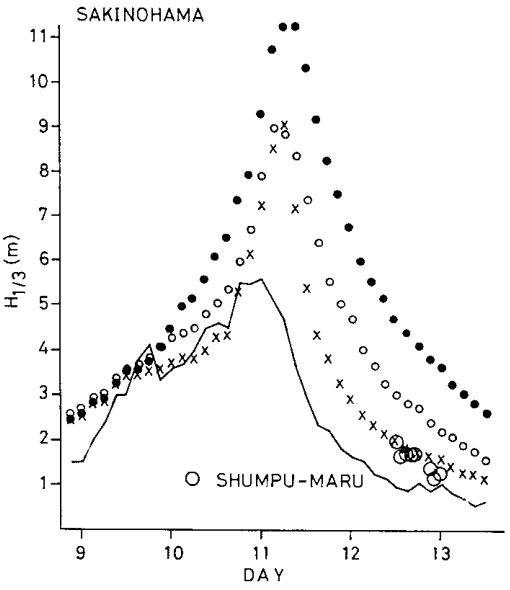

Fig. 5. Observed and computed significant wave heights at Sakinohama, the grid point (14, 13) and those observed on the R. V. *Shumpu Maru* at stations marked by crosses in Fig. 2. The symbols are the same as in Fig. 4.

such as typhoons. It is also worth noting that the energy dissipation term tuned by the data at Buoy No. 3 and at the stations of the R.V. *Shumpu Maru* also gives the most reasonable wave height at all of the other observation stations.

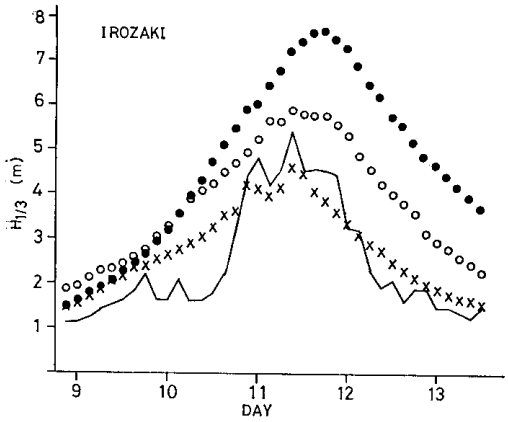

Fig. 6. Observed and computed significant wave heights at Irozaki and the grid point (18, 12). The symbols are the same as in Fig. 4.

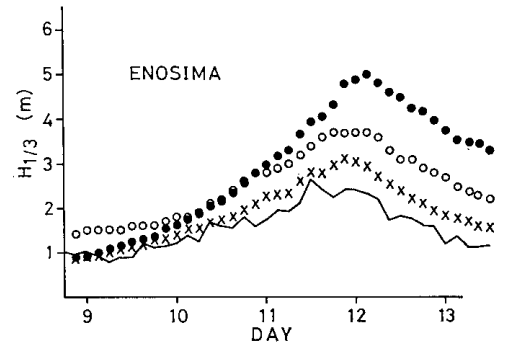

Fig. 7. Observed and computed significant wave heights at Enoshima and the grid point. (21, 7). The symbols are the same as in Fig. 4.

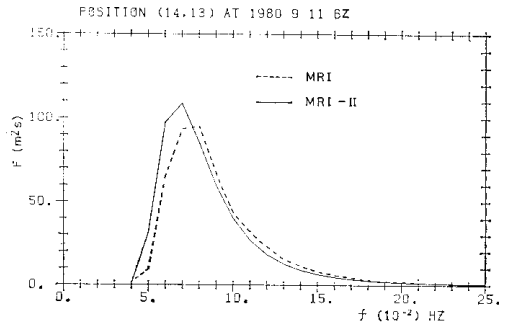

Fig. 8. One-dimensional spectra for MRI and MRI-II at the grid point (14, 13) at 06z 11 September in the period of high waves.

One-dimensional spectra computed by MRI and MRI-II (from now on MRI-II refers to MRI-II with wave breaking effects included unless otherwise noted) at the grid point (14, 13) at 06 z 11 September are shown in Fig. 8 and those at 18 z 12 September in Fig. 9. The agreement of the spectra at 06 z is remarkable, while for the spectra at 18 z MRI gives a large energy peak in the frequency range from 0.11 to 0.14 Hz, but MRI-II yields no significant energy peak. The spectra observed by the R.V. *Shumpu Maru* and at Sakinohama at the same time are shown in Fig. 10. It is natural that the total energy predicted by MRI-II and shown in Fig. 9 agree with the observations of the R.V. *Shumpu Maru* because MRI-II was tuned by means of observations around this station. However, it is remarkable that both one-dimensional spectra have almost the same form.

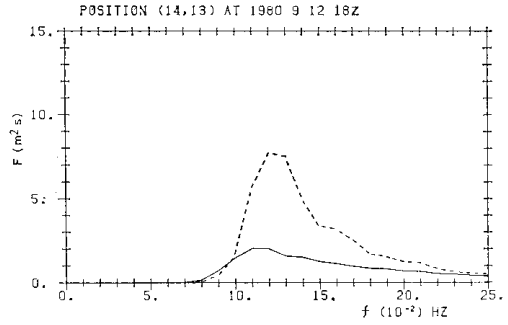

Fig. 9. Same as Fig. 8 except that the time is 18z 12 September during the decay stage of waves.

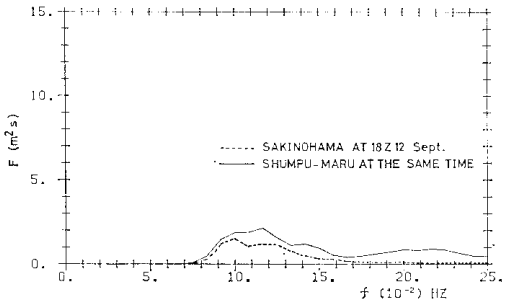

Fig. 10. One-dimensional spectra observed by the R. V. *Shumpu Maru* at K4 (see Fig. 2) and at Sakinohama.

In Fig. 11, the two-dimensional forms of the spectra in Fig. 9 are normalized by dividing by their maximum value and then contoured at an interval of 0.1. There is a large difference in the directional distribution of the energy between MRI and MRI-II. For the spectrum of MRI, wave energy is travelling mainly toward

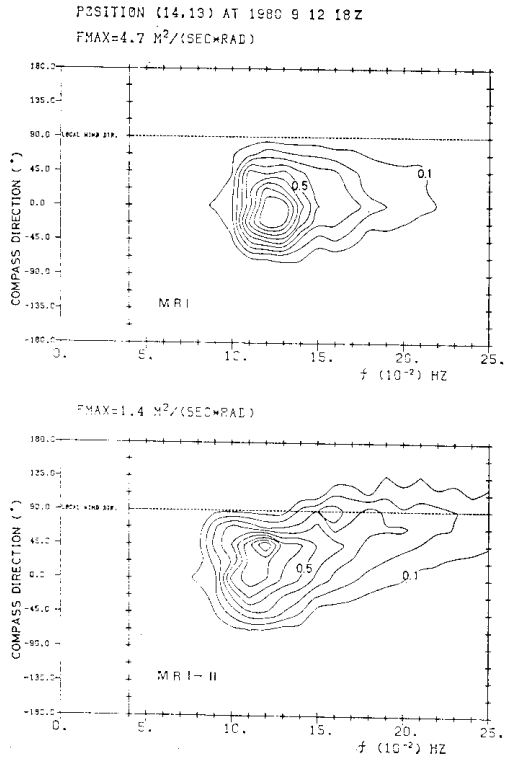

Fig. 11. Two-dimensional spectra normalized by the maximum value. The one-dimensional forms of these spectra are shown in Fig. 9. The upper figure is for MRI and the lower is for MRI-II. The ordinate shows compass direction in degrees.

the NNW and N. On the other hand, the main energy for MRI-II is toward the NE. In other words, the swell travelling N or NNW in MRI is considerably dissipated in MRI-II.

Figure 5 shows that the waves observed at Sakinohama are lower than those observed on the R.V. *Shumpu Maru* as well as being lower than all hindcasted waves after September 11. The observation station at Sakinohama is located 2 km off the east of a cape as shown in Fig. 2, and it lies on a compass bearing of 20° from the tip of the cape. Therefore a wave component travelling eastward along a direction greater than 20° does not reach the station directly.

Let *Ed* be the sum of the energy running in directions which can reach the station directly. The mean direction of the wave energy at the grid point (14, 13) and the ratio of *Ed* to the total energy are shown in Fig. 12. After 09 z

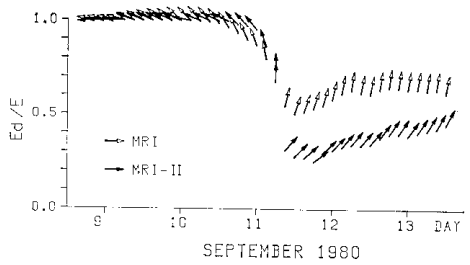

Fig. 12. Mean directions of wave energy at the grid point (14, 13) and the ratios of *Ed* to total energy *E* for MRI and MRI-II. The mean wave direction is indicated by an arrow and upward is north. The position of the tail of the arrow in the ordinate indicates the energy ratio.

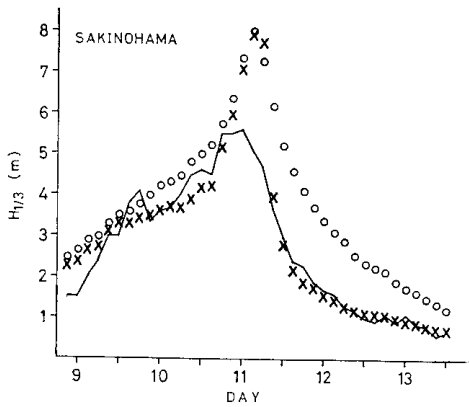

Fig. 13. Wave heights corresponding to *Ed* and the observations at Sakinohama. The symbols are the same as in Fig. 4.

11 September there is a difference between MRI and for MRI-II in the computed mean wave directions as well as in the energy ratio. The cape shuts out about 50 % of the wave energy for MRI and about 70 % for MRI-II after 09 z 11 September.

Wave height at Sakinohama corresponding to *Ed* is shown in Fig. 13. The agreement between the results of MRI-II and the observations at Sakinohama is remarkable after 09 z 11 September. This shows that the directional properties of waves obtained by MRI-II are more reliable than those of MRI. The results also show that the difference in wave height at Sakinohama and the observation stations of the R.V. *Shumpu Maru* is due to the shade effect of the cape.

Even though the figure shows a large dis-

crepancy in wave height between observations and the computations during the period from 00 z 11 to 06 z 11 September, I believe this discrepancy is caused by some error in estimation of the wind field rather than being due to a deficiency in the wave models, because both models yield almost the same results during this period in spite of the fact that they are based on different pictures of the spectral energy balance. Furthermore, the results of MRI-II are in good agreement with observations at all observation stations throughout the period of hindcast. However I cannot prove this view at present, because of a lack of appropriate wind data from the central region of the typoon over the sea.

Wave heights and one-dimensional spectra hindcasted by MRI agree with those of MRI-II for very high wave conditions. At the decay stage of waves, however, the wave height, the one-dimensional wave spectrum and the two-dimensional wave spectrum are hindcasted more accurately by MRI-II than by MRI. It can be concluded, therefore, that the explicit representation of S_{ds} due to wave breaking in MRI-II is very successful. It can be also concluded that the dissipation function S_{ds} can be applied without reference to the varying conditions of wind and waves during practical use. This conclusion is reached for the following reasons: (1) since over-saturated components appear most prominently in wind fields where wind rapidly changes speed and direction both in time and space, a hindcast of waves due to a typhoon is one of the most extreme but realistic tests of S_{ds} for over-saturated components, (2) the dissipation term tuned by wave heights observed only at two points gives not only reasonable wave heights at all other observation stations but also yields reasonable directional property of waves.

4. Basic performance of MRI-II

To test the basic performance of MRI-II, a numerical experiment which corresponds to Case II of the SWAMP experiment was carried out. The experiment examined the growth of a wave field in a square sea 1,000×1,000 km in size for a uniform, stationary wind of 20 m sec^{-1} blowing orthogonally off a straight shore. The sea state is initially calm. For a large fetch the evolution of the wave field with time provides a duration-limited growth curve of the model, while for a large duration the dependence of the wave field on the distance off-shore presents a fetch-limited growth curve.

Since the energy propagation term is negligibly small for a large fetch, the duration-limited growth curve for the peak frequency agrees well with the theoretical curve of Eq. (7), as would expected. The substitution of the values of C_1 and C_2 into Eq. (2′) gives the equation

$$d\sigma_p^{*-3}/dx^* = 5.51\times10^{-3} \times[1-erf(4.59\times10^{-2}\,\sigma_p^{*-1})], \quad (11)$$

which controls the fetch limited growth of waves for a steady state. On the other hand, the waves of this numerical experiment under steady fetch-limited conditions are determined by two terms of Eq. (1); one is the energy input S_{net} controlled by Eqs. (7) and (8) and the other is the advection term which is calculated numerically for each two-dimensional spectral component. Therefore, the agreement of the fetch-limited growth curve of the experiment for $f_p^*=\sigma_p^*/2\pi$ and that obtained from Eq. (11) shown in Fig. 14 is very important, because it shows that not only our numerical scheme for energy propagation but also the matching of the two-dimensional representation of wave energy and the parametric representation of windsea are satisfactory.

The duration-limited growth curves and the fetch-limited ones for MRI were not well defined, and it can also be seen from this figure that this weak point of MRI is completely over-

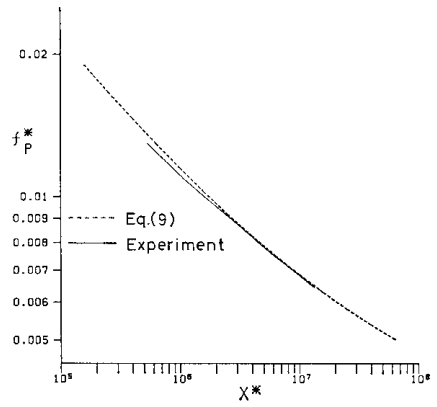

Fig. 14. Non-dimensional fetch-limited growth curves of MRI-II for the peak frequency.

come in MRI-II, and the main purpose of this work has been accomplished.

5. Conclusions

MRI-II is designed to overcome a weak point of MRI without losing its merits; namely, the inferior representation of the shape of the windsea spectra at early stages of windsea growth. For this purpose, a one-parameter representation of windsea is incorporated into MRI that calculates energy propagation based on a two-dimensional spectral representation of wind waves. The weak point of MRI is overcome by the one-parameter representation, *i.e.*, MRI-II greatly excels over MRI in describing both the fetch-limited and duration-limited growth stages of windsea.

Hypothetical assumptions are also introduced into MRI-II to describe wave breaking effects for over-saturated components. The numerical constant required in the assumptions is determined through trial test runs for a hindcast. As a result of incorporation of these wave breaking effects, MRI-II gives more reasonable estimates not only of the wave height and the one-dimensional spectrum but also the two-dimensional spectrum. Thus, MRI-II also outperforms MRI in applications to actual wind fields.

Taking into account the accuracy and the time and spatial sparseness of available wind data for wave prediction, the performance of MRI-II is remarkably good.

Acknowledgements

The author would like to acknowledge the continuing guidance and encouragement of Prof. Y. Toba of Tohoku University. He is grateful to the officials of the Maritime Meteorological Division of J.M.A. for providing the wind data on typhoon ORCHID and their hindcast results obtained using MRI. He is also indebted to Dr. Iida, head of Oceanographical Research Division of M.R.I. and Dr. Isozaki, chief of the Second Research Laboratory of the Division for their support and encouragement.

References

Hasselmann, K. (1962): On the non-linear energy transfer in a gravity wave spectrum. Part. 1. J. Fluid Mech., **12**, 481-500.

Hasselmann, K., T. P. Barnett, E. Bouws, H. Carlson, D. E. Cartwright, K. Enke, J. A. Ewing, H. Gienapp, D. E. Hasselmann, P. Kuseman, A. Meerburg, P. Muller, D. J. Olbers, K. Richter, W. Sell and H. Walden (1973): Measurements of wind-wave growth and swell decay during the Joint North Sea Wave Project (JONSWAP). Dt. Hydrogr. Z., Suppl. A. 8, No. 12, 95pp.

Isozaki, I. and T. Uji (1973): Numerical prediction of ocean waves. Papers in Met. and Geophys., **24**, 207-232.

Mitsuyasu, H., F. Tasai, T. Suhara, S. Mizuno, M. Ohkusu, T. Honda and K. Rikiishi (1980): Observation of the power spectrum of ocean waves using a clover-leaf buoy. J. Phys. Oceanogr., **10**, 286-296.

The SWAMP group (1982a): The Sea Wave Modelling Project. Part 1. Principal results and conclusions. Proc. Symp. on Wave Dynamics and Radio Probing of Ocean Surface, Miami, 1981.

The SWAMP Group (1982b): The Sea Wave Modelling Project. Part 2. Compilation of results. Proc. Symp. on Wave Dynamica and Radio Probing of Ocean Surface, Miami, 1981.

Toba, Y. (1972): Local balance in the air-sea boundary processes. Part 1. J. Oceanogr. Soc. Japan, **28**, 15-26.

Toba, Y. (1973a): Local balance in the air-sea boundary processes. Part 2. J. Oceanogr. Soc. Japan, **29**, 24-29.

Toba, Y. (1973b): Local balance in the air-sea boundary processes. Part 3. J. Oceanogr. Soc. Japan, **29**, 39-50.

Toba, Y. (1978): Stochastic form of the growth of wind waves in a single-parameter representation with physical implications. J. Phys. Oceanogr., **8**, 494-507.

Toba, Y. (1979): Study on wind waves as a strong nonlinear phenomenon. 12th Symp. on Naval Hydrodynam., National Acad. Sci., Washington, D. C., 521-540.

Uji. T. (1975): Numerical estimation of the sea waves in a typhoon area. Papers in Met. and Geophys., **26**, 199-217.

Uji. T. and I. Isozaki (1972): The calculation of wave propagation in the numerical prediction of ocean waves. Papers in Met. and Geophys., **23**, 347-359.

Wilson, B. W. (1965): Numerical prediction of ocean waves in the North Atlantic for December, 1959. Dt. Hydrogr. Z., **18**, 114-130.

波浪予報モデル MRI-II

宇 治 豪*

要旨: 波浪に対する5つのエネルギー輸送過程を組み込んだ波浪予報モデルを作成した.

この5つの過程とは, 順風によるエネルギーの入力, 共鳴相互作用による風波の成分波間における非線形エネルギー輸送, 砕波と粘性による散逸および逆風の効果である.

このモデルでは成長段階の風波を単一パラメータで表現しているので, 非線形エネルギー輸送と風からの入力は同時にかつ陰に含まれている. 風波のスペクトル形の相似性, 波高と周期の間の鳥羽による3/2乗則, ピーク周波数に対する鳥羽の発達式および充分発達した風波のPierson-Moskowitz のスペクトルが単一パラメータ表現の具体的内容である.

うねりとうねり, または, うねりと風波の間の共鳴相互作用はこの形式では表現できないので無視してある.

また砕波が波高の2乗に比例する大きさの水塊のエネルギー散逸を伴うと仮定して, その効果をモデルに取入れた. この仮説による砕波の表現に含まれる未定常数は北西太平洋における波浪の追算により決定した.

この新しいモデルで追算した波高, 1次元スペクトルおよび2次元スペクトルは古いモデル MRI で追算した結果より観測結果によく合うことがわかった.

* 気象研究所
〒305 茨城県筑波郡谷田部町長峰 1-1